Combination of the Replica-Exchange Monte Carlo Method and the Reference Interaction Site Model Theory for Simulating a Peptide Molecule in Aqueous Solution

Ayori Mitsutake,*,† Masahiro Kinoshita,‡ Yuko Okamoto,§,|| and Fumio Hirata§,||

Department of Physics, Faculty of Science and Technology, Keio University, Yokohama, Kanagawa 223-8522, Japan, Advanced Energy Utilization Division, Institute of Advanced Energy, Kyoto University, Uji-shi, Kyoto 611-0011, Japan, Department of Theoretical Studies, Institute for Molecular Science, Okazaki, Aichi 444-8585, Japan, and Department of Functional Molecular Science, The Graduate University for Advanced Studies, Okazaki, Aichi 444-8585, Japan

Received: May 20, 2004; In Final Form: September 22, 2004

This article reports the first attempt to combine the replica-exchange Monte Carlo method and the reference interaction site model (RISM) theory for simulating a peptide molecule in aqueous solution. The energy function is the sum of the conformational energy and the solvation free energy. The solvation free energy for a fixed conformation of the peptide molecule is calculated using the RISM theory. The replica-exchange method is modified so that the dependence of the energy function on the temperature can be incorporated. The effectiveness of the combined approach is demonstrated for Met-enkephalin in water. It is argued that the number of replicas required for a peptide molecule immersed in water is drastically reduced by employing the combined approach. Solvation properties and free energy surfaces of Met-enkephalin in water are discussed.

1. Introduction

The conformational stability of proteins is determined by the competition of the conformational energy, chain entropy, and hydration free energy. Usual thermal denaturation is caused by the increase in chain entropy as the temperature is raised, and it is the general nature of polymers. However, some proteins are known to denaturate when the temperature is decreased, that is, "cold denaturation".[1] The unique features of proteins can never be understood without accounting for the role of the hydration free energy in determining the stability of proteins. Although the continuum model has been widely employed in the literature in order to explain the solvation effects, the method does not account for the hydrophobicity, which is essential in determining protein stability. Therefore, the solvent should be treated on the atomic level.

In usual simulations, a peptide molecule and sufficiently many surrounding solvent molecules are treated simultaneously. However, the number of solvent molecules required becomes huge for a large peptide or a protein. Moreover, in the usual simulations with explicit molecules, the treatment of a mixture of more than one solvent species, such as a saline solution, is nontrivial. The reference interaction site model (RISM) theory[2−4] can treat not only an infinite number of solvent molecules but also the salt effects. The RISM theory has been developed from the statistical mechanics of molecular liquids. This theory can estimate the solvation free energy of a solute molecule with fixed structures in infinite dilution. Therefore, the RISM theory is particularly suitable for these treatments. We developed an algorithm for solving the full RISM equations for the system of a solute molecule with many atoms in water and salt solution that is more robust and orders of magnitude faster than the conventional one.[5,6] In our earlier work, we analyzed the solvation structure and conformational stability of a pentapeptide Met-enkephalin with the RISM theory.[7] We also reported results of the first attempt to combine Monte Carlo (MC) simulated annealing and the RISM theory.[8,9] The combined program was tested for Met-enkephalin[8] and the C-peptide fragment of ribonuclease A[9] in water. These results are summarized in ref 5.

Besides the solvation theory, effective simulation algorithms are also important for studying protein folding and stability. The generalized-ensemble algorithm is one of the most powerful configurational space sampling methods (for recent reviews, see refs 10 and 11). This method is based on non-Boltzmann probability weight factors so that a random walk in potential energy space may be realized. The random walk allows the simulation to escape over any energy barrier and to sample a much wider configurational space than by conventional methods. From this simulation run, one can not only locate the energy global minimum but also calculate the canonical-ensemble average of any physical quantity at any temperature. One of the most well-known generalized-ensemble algorithms for simulating protein systems is perhaps the multicanonical algorithm (MUCA).[12,13] Another powerful configurational space sampling method is the replica-exchange method (REM).[14−16] A number of new generalized-ensemble algorithms that are related to REM have been developed.[17−23]

In the previous work, we combined the RISM theory and multicanonical algorithm and performed a simulation of Met-enkephalin in aqueous solution.[24] In the RISM theory, the solvation free energy depends on the temperature. However, the multicanonical algorithm cannot treat temperature-dependent energy. Thus, in the previous multicanonical simulation, we only used the solvation free energy at a room temperature as the solvent effects. In the present paper, we try to include the effects of the temperature dependence of the solvation free energy. For

* Author to whom correspondence should be addressed. E-mail: ayori@rk.phys.keio.ac.jp.
† Keio University.
‡ Kyoto University.
§ Institute for Molecular Science.
|| The Graduate University for Advanced Studies.

10.1021/jp047824d CCC: $27.50
Published on Web 11/12/2004

this purpose, we have to modify the formulation of the replica-exchange method (the same modification of REM was used in ref 25). We combine this modified replica-exchange method and the RISM theory. We applied this hybrid simulation method to the pentapeptide Met-enkephalin and tested its effectiveness. We obtained the distribution functions and thermodynamic quantities as functions of temperature. The free energy surface was also analyzed, in which the principal component analysis[26−30] (see also ref 31) was employed. We found that the number of required replicas is much smaller than in the regular simulation with explicit solvent molecules. This is a great advantage when applying the present method to a larger system.

The present article is organized as follows. In section 2.1, we outline the hybrid method with the RISM theory and molecular simulation. In section 2.2, we briefly explain the RISM theory. In section 2.3, we explain the modified replica-exchange method. In section 2.4, we briefly describe the principal component analysis. In section 2.5, the computational details are given. In section 3, we present the results of the simulation. Section 4 is devoted to conclusions.

2. Methods

2.1. Hybrid RISM/MC Method. In usual simulations, the energy function is an instant value of the potential energy for the entire system configuration. In our hybrid simulations,[6−9,24] the total energy function E_T is given by the sum of the conformational energy E_C and the solvation free energy E_{SOL} of the biomolecule in a fixed conformation

$$E_T = E_C + E_{SOL} \tag{1}$$

Here, the conformational energy E_C consists, for example, of an electrostatic term, a Lennard-Jones term, and a torsion-energy term. In the present work, we use the RISM theory to calculate E_{SOL}. The total energy function in eq 1 is different from the usual potential energy, because we use the solvation free energy E_{SOL}. We refer to the total energy function as the "solvent-induced potential".[5]

Let us consider a system comprising a biomolecule with N_S atoms and L solvent molecules. Each solvent molecule has N_V atoms, and N_VL solvent atoms constitute the solvent. In the usual computer simulations, the energy function is the potential energy of the whole system. The total potential E_{TOT} is given by

$$E_{TOT} = E_C + E_{CV} + E_V \tag{2}$$

where E_C is the conformational energy as in eq 1, E_{CV} is the solute−solvent interaction energy, and E_V is the solvent−solvent interaction energy. The partition function Z of the system can be written as

$$Z = \int\int \mathrm{d}\boldsymbol{r}_C\, \mathrm{d}\boldsymbol{r}_V \exp\{-\beta(E_C + E_{CV} + E_V)\} \tag{3}$$

where $\beta = 1/k_BT$, k_B is the Boltzmann constant, and T is the absolute temperature. The integration is performed with respect to positions $\boldsymbol{r}_C$ of the N_S solute atoms and $\boldsymbol{r}_V$ of the N_VL solvent atoms. The ensemble average of a physical quantity $A(\boldsymbol{r}_C,\boldsymbol{r}_V)$, which represents the instant value for a system configuration, is given by

$$\langle A\rangle_T = \frac{1}{Z}\int\int \mathrm{d}\boldsymbol{r}_C\, \mathrm{d}\boldsymbol{r}_V\, A(r_C,r_V) \exp\{-\beta(E_C + E_{CV} + E_V)\} \tag{4}$$

The partition function Z_V of the pure solvent of N_VL solvent atoms is written as

$$Z_V = \int \mathrm{d}\boldsymbol{r}_V \exp(-\beta E_V) \tag{5}$$

Using eq 5, we rewrite eq 4 as

$$\langle A\rangle_T = \frac{Z_V}{Z} I_1 \tag{6}$$

$$I_1 = \frac{\int \mathrm{d}\boldsymbol{r}_C\, \mathrm{d}\boldsymbol{r}_V\, A(\boldsymbol{r}_C,\boldsymbol{r}_V) \exp\{-\beta(E_C + E_{CV} + E_V)\}}{\int \mathrm{d}\boldsymbol{r}_V \exp(-\beta E_V)} \tag{7}$$

We now consider the case in which the physical quantity A is a function of only $\boldsymbol{r}_C$; examples are the conformational energy and the end-to-end distance of the biomolecule. I_1 can then be written as

$$I_1 = \frac{\int \mathrm{d}\boldsymbol{r}_C\, [A(\boldsymbol{r}_C) \exp(-\beta E_C)\int \mathrm{d}\boldsymbol{r}_V \exp\{-\beta(E_{CV} + E_V)\}]}{\int \mathrm{d}\boldsymbol{r}_V \exp(-\beta E_V)} \tag{8}$$

Because we are mainly concerned with a biomolecule conformation in solvent, this is not a significant limitation. Note that E_{CV} in eq 8 is dependent on both $\boldsymbol{r}_C$ and $\boldsymbol{r}_V$. We define I_2 by

$$I_2 = \int \mathrm{d}\boldsymbol{r}_V \exp\{-\beta(E_C + E_{CV} + E_V)\} \tag{9}$$

I_2 is the integration over positions of the N_VL solvent atoms with fixed positions of the N_S atoms in the biomolecule and is related to the excess free energy F_{ex} of the system comprising the biomolecule in a fixed conformation and the solvent

$$I_2 = V^{N_VL} \exp(-\beta F_{ex}) \tag{10}$$

where V is the volume of the entire system. F_{ex} should be distinguished from A_{ex}, which is the usual excess free energy of the system where the conformation of the biomolecule is not fixed

$$Z = \int \mathrm{d}\boldsymbol{r}_C\, \mathrm{d}\boldsymbol{r}_V \exp\{-\beta(E_C + E_{CV} + E_V)\} \tag{11}$$

$$= \int \mathrm{d}\boldsymbol{r}_C\, I_2 \tag{12}$$

$$= V^{N_VL+N_S} \exp(-\beta A_{ex}) \tag{13}$$

Equating the right-hand sides of eqs 9 and 10 gives

$$\int \mathrm{d}\boldsymbol{r}_V \exp\{-\beta(E_{CV} + E_V)\} = V^{N_VL} \exp\{-\beta(F_{ex} - E_C)\} \tag{14}$$

The denominator of eq 8 is related to the excess free energy F_{ex0} of the pure solvent of N_VL atoms by

$$\int \mathrm{d}\boldsymbol{r}_V \exp(-\beta E_V) = V^{N_VL} \exp(-\beta F_{ex0}) \tag{15}$$

The solvation free energy E_{SOL} in eq 1 can be identified as

$$E_{SOL} = F_{ex} - E_C - F_{ex0} \tag{16}$$

In the following, we show that eq 16 gives rise to a proper Boltzmann factor for sampling conformational space of a biomolecule in solvent accounting for the solvation free energy. It should be emphasized that E_{SOL} is dependent on $\boldsymbol{r}_C$ and eq 16 differs from the usual definition of the solvation free energy where the conformation of the biomolecule is not fixed. Substituting eqs 14 and 15 into eq 8 and using eq 16 yields

$$I_1 = \int d\mathbf{r}_C\, A(\mathbf{r}_C) \exp\{-\beta(E_C + E_{SOL})\} \tag{17}$$

In a similar fashion, we obtain

$$\frac{Z_V}{Z} = \frac{1}{\int d\mathbf{r}_C \exp\{-\beta(E_C + E_{SOL})\}} \tag{18}$$

Substituting eqs 17 and 18 into eq 7 yields

$$\langle A \rangle_T = \frac{\int d\mathbf{r}_C\, A(r_C) \exp\{-\beta(E_C + E_{SOL})\}}{\int d\mathbf{r}_C \exp\{-\beta(E_C + E_{SOL})\}} \tag{19}$$

The "exact" equation, eq 19, implies that the ensemble average of $A(\mathbf{r}_C)$ can be calculated using the integration over the conformation of the biomolecule alone when the energy function in the Boltzmann factor is taken to be the solvent-induced potential $E_T = E_C + E_{SOL}$ in eq 1.

E_T is equivalent to $[F_{ex} - F_{ex0}]$ where F_{ex} is the excess free energy of the system comprising the biomolecule in the fixed conformation and the solvent and F_{ex0} is the excess free energy of pure solvent. We emphasize that the solvent is always in equilibrium with each conformation of biomolecule sampled.

After performing the simulation with the weight factor $W(\mathbf{r}_C,T) = \exp[-\beta\{E_T(\mathbf{r}_C,T)\}]$, we can exactly obtain the average of physical quantity $A(\mathbf{r}_C)$ by

$$\langle A \rangle_T = \frac{\int d\mathbf{r}_C\, A(r_C) W(r_C,T)}{\int d\mathbf{r}_C\, W(r_C, T)} = \frac{1}{N_{SIM}} \sum_{i=1}^{N_{SIM}} A_i(\mathbf{r}_C) \tag{20}$$

where N_{SIM} is the number of samples taken.

2.2. Reference Interaction Site Model. The solvation free energy E_{SOL} is calculated by the RISM theory.[5,6−9] It is assumed that the solute is present in the solvent at the infinite-dilution limit. The calculation process is split into two steps where bulk solvent (step 1) and solvent near a solute molecule (step 2) are successively treated. The basic equations for step 2 comprise the site−site Ornstein−Zernike (SSOZ) relation and the hypernetted-chain (HNC) closure equation. Let the subscript S and the subscript V denote the solute molecule and the solvent molecule, respectively. The model of the water molecule that we adopted is the SPC/E model.[32] Suppose that the solute molecule has N_S atomic sites and the solvent molecule has N_V atomic sites ($N_V = 3$ for water). The SSOZ relation in the Fourier space is given by

$$\boldsymbol{\eta}_{sv} = \boldsymbol{w}_{sv}\boldsymbol{c}_{sv}\boldsymbol{H}_{vv} - \boldsymbol{c}_{sv} \tag{21}$$

$$\boldsymbol{\eta}_{sv} = \boldsymbol{h}_{sv} - \boldsymbol{c}_{sv} \tag{22}$$

$$\boldsymbol{H}_{vv} = \boldsymbol{w}_{vv} + \boldsymbol{\rho}_v \boldsymbol{h}_{vv} \tag{23}$$

where $\boldsymbol{H}_{vv}$, $\boldsymbol{\eta}_{sv}$, and $\boldsymbol{w}_{ss}$ are $N_V \times N_V$, $N_S \times N_V$, and $N_S \times N_S$ matrices, respectively, $\boldsymbol{\rho}_v$ is the matrix of the number density of the solvent, $\boldsymbol{h}$ is the matrix of the site−site intermolecular total correlation functions, $\boldsymbol{c}$ is the matrix of the site−site intermolecular direct correlation functions, and $\boldsymbol{w}$ is the intramolecular correlation matrix. $\boldsymbol{H}_{vv}$ is calculated in step 1 and is part of the input data for step 2. The HNC closure equation is given by

$$c_{AB}(r) = \exp\{-u_{AB}(r)/k_BT + \eta_{AB}(r)\} - \eta_{AB}(r) - 1 \tag{24}$$

$$A = 1,..., N_S; \quad B = 1,..., N_V$$

$$\eta_{AB}(r) = h_{AB}(r) - c_{AB}(r) \tag{25}$$

where $u_{AB}(r)$ is the site−site interaction potential energy. A is an atomic site in the solute molecule, and B is an atomic site in the solvent molecule. After the site−site intermolecular correlation functions $h_{AB}(r)$ and $c_{AB}(r)$ are obtained by solving the RISM-HNC equations, the solvation free energy E_{SOL} for the solute molecule is calculated from[33]

$$E_{SOL} = 4\pi k_B T \int_0^\infty F(r) r^2\, dr \tag{26}$$

$$F(r) = \sum_{A=1}^{N_S} \sum_{B=H,O} \rho_B \left[\frac{h_{AB}(r)^2}{2} - c_{AB}(r) - \frac{h_{AB}(r) c_{AB}(r)}{2} \right] \tag{27}$$

$$\rho_H = 2\rho_V, \quad \rho_O = \rho_V \tag{28}$$

where ρ are number densities. The dimensionless number density of water $\rho_V d^3$ ($d = 2.8$ Å) is 0.7317.

2.3. Replica-Exchange Method with Temperature-Dependent Potential Energy. In this subsection, we describe the replica-exchange method with a temperature-dependent energy function.

The generalized ensemble for REM consists of M noninteracting copies of the original system in the canonical ensemble at M different temperatures T_m ($m = 1, ..., M$). We arrange the replicas so that there is always exactly one replica at each temperature. Then, there is a one-to-one correspondence between replicas and temperatures; the label i ($i = 1,..., M$) for replicas is a permutation of the label m ($m = 1, ..., M$) for temperatures, and vice versa

$$\begin{cases} i = i(m) \equiv f(m) \\ m = m(i) \equiv f^{-1}(i) \end{cases} \tag{29}$$

where $f(m)$ is a permutation function of m and $f^{-1}(i)$ is its inverse.

Let $X = \{x_1^{[i(1)]}, ..., x_M^{[i(M)]}\} = \{x_{m(1)}^{[1]}, ..., x_{m(M)}^{[M]}\}$ stand for a "state" in this generalized ensemble. The state X is specified by the M sets of coordinates $x_m^{[i]}$ in replica i at temperature T_m. In the replica-exchange simulation with the solvent-induced potential, the weight factor for the state $X = \{..., x_m^{[i]}, ...\}$ is given by the product of $\exp[-\beta\{E_T(\mathbf{r}_C,T)\}]$ for each replica

$$W_{REM}(X) = \prod_{i=1}^{M} \exp(-\beta_{m(i)}\{E_T(\mathbf{r}_C^{[i]}, T_{m(i)})\}) \tag{30}$$

$$= \prod_{m=1}^{M} \exp(-\beta_m\{E_T(\mathbf{r}_C^{[i(m)]}, T_m)\}) \tag{31}$$

where $i(m)$ and $m(i)$ are the permutation functions in eq 29 and $\mathbf{r}_C^{[i]}$ is a coordinate of a protein in replica i at temperature T_m. Note that the temperature dependence of the total energy E_T comes from the solvation free energy E_{SOL} (see eqs 24, 26, and 27).

We now consider exchanging a pair of replicas, i and j, which are at temperatures T_m and T_n, respectively, $X = \{..., x_m^{[i]}, ..., x_n^{[j]}, ...\} \rightarrow X' = \{..., x_m^{[j]}, ..., x_n^{[i]}, ...\}$. From the condition of detailed balance of replica exchange, we obtain the following relation

$$W_{REM}(X) w(X \rightarrow X') = W_{REM}(X') w(X' \rightarrow X) \tag{32}$$

where $w(X \rightarrow X')$ is the transition probability of going from

state X to state X' and $w(X' \rightarrow X)$ is the transition probability of going from state X' to state X. From eqs 31 and 32, we have (see also refs 18, 19, 21, and 22)

$$\frac{w(X \rightarrow X')}{w(X' \rightarrow X)} = \exp(-\Delta) \tag{33}$$

where

$$\Delta = \beta_m\{E_T(\mathbf{r}_C^{[j]},T_m) - E_T(\mathbf{r}_C^{[i]},T_m)\} - \beta_n\{E_T(\mathbf{r}_C^{[j]},T_n) - E_T(\mathbf{r}_C^{[i]},T_n)\} \tag{34}$$

Here, $\mathbf{r}_C^{[i]}$ and $\mathbf{r}_C^{[j]}$ are the set of the coordinates of atoms in replica i and replica j, respectively. We remark that when E_T is independent of temperature, we have

$$\Delta = (\beta_m - \beta_n)(E_T(\mathbf{r}_C^{[j]}) - E_T(\mathbf{r}_C^{[i]})) \tag{35}$$

which we usually use in the regular replica-exchange simulation.

As a result, the transition probability of the replica-exchange process is given by the Metropolis criterion

$$w(X \rightarrow X') = \begin{cases} 1 & \text{for } \Delta \le 0 \\ \exp(-\Delta) & \text{for } \Delta > 0 \end{cases} \tag{36}$$

where Δ is given by eq 34. Without loss of generality we can assume $T_1 < T_2 < ... < T_M$. A simulation of REM is then realized by alternately performing the following two steps:

1. Each replica in canonical ensemble of the fixed temperature is simulated *simultaneously* and *independently* for a certain MC steps.

2. A pair of replicas at neighboring temperatures, say $x_m^{[i]}$ and $x_{m+1}^{[j]}$, are exchanged with the probability $w(X \rightarrow X')$ in eq 36. Note that in step 2 we exchange only pairs of replicas corresponding to neighboring temperatures.

Some remarks are now in order. For the replica exchange to occur with sufficiently high frequency, the acceptance probability $\exp(-\Delta)$ in eq 36 for replica exchange must be large enough. In the regular replica-exchange method, if the energy difference between two system configurations, $E_T(\mathbf{r}_C^{[j]}) - E_T(\mathbf{r}_C^{[i]})$, is large, then the difference of neighboring temperatures, $T_{m+1} - T_m$, should be set sufficiently small (see eq 35). A smaller difference in the temperature leads to a larger number of required replicas. The problem is that even in gas phase the energy difference increases as the size of the biomolecule becomes larger. Matters get worse when the biomolecule is immersed in solvent. Due to the large number of solvent molecules, not only the absolute values of the energy function but also the relative values among different system configurations are greatly magnified. As a consequence, the energy difference becomes much larger than in gas phase, and the number of replicas required increases as the size of the biomolecule becomes larger. The greatest advantage of the hybrid simulation is a drastic reduction in the number of replicas required. As discussed in detail in the following section, it has been found from the present simulation of Met-enkephalin in water that the solvation free energy scaled by k_BT is not significantly dependent on the temperature. It follows that the absolute values of $\beta_m\{E_T(\mathbf{r}_C^{[j]},T_m) - E_T(\mathbf{r}_C^{[i]},T_m)\}$ and $\beta_n\{E_T(\mathbf{r}_C^{[j]},T_n) - E_T(\mathbf{r}_C^{[i]},T_n)\}$ are always comparable with each other, and Δ in eq 34 never takes a large positive value even when there is a large difference between T_m and T_n. In the case of Met-enkephalin immersed in water, only four replicas were sufficient to guarantee high replica-exchange frequency.

2.4. Principal Component Analysis. The principal component analysis (PCA) is used to extract a dynamically relevant motion of a protein from simulation results.[26−31] We consider a protein consisting of N atoms. We extract N_D data points from the MC trajectory of coordinates distributed in a $3N$-dimensional space. A configuration corresponds to a single vector $\mathbf{X}$ with $3N$ components. This is often represented by the mass-weighted coordinate: $\mathbf{X} = [X_1, X_2, X_3, ..., X_{3N-2}, X_{3N-1}, X_{3N}] = [\sqrt{m_1}x_1, \sqrt{m_1}y_1, \sqrt{m_1}z_1, \cdots, \sqrt{m_N}x_N, \sqrt{m_N}y_N, \sqrt{m_N}z_N]$, where x_k, y_k, and z_k are the Cartesian coordinates of the kth atom. The standard deviation of the mass-weighted coordinates $\mathbf{X}(t_a)$ at time t_a from their time averages $\langle\mathbf{X}\rangle$ along a normalized unit vector $\mathbf{v}$ is given by

$$R = \frac{1}{N_D}\sum_{t_a=1}^{N_D}\{(\mathbf{X}(t_a) - \langle\mathbf{X}\rangle)\cdot\mathbf{w}\}^2 \tag{37}$$

$$= \mathbf{w}^T\mathbf{C}\mathbf{w} \tag{38}$$

Here,

$$\langle\mathbf{X}\rangle = \frac{1}{N_D}\sum_{t_a=1}^{N_D}\mathbf{X}(t_a) \tag{39}$$

and the $3N \times 3N$ variance−covariance matrix $\mathbf{C}$ has the following components

$$C_{ij} = \frac{1}{N_D}\sum_{t_a=1}^{N_D}(X_i(t_a) - \langle X_i\rangle)(X_j(t_a) - \langle X_j\rangle) \tag{40}$$

where X_i is the ith component of the vector $\mathbf{X}$ and the translational and rotational motions have been removed. The vector in which R has the largest value corresponds to the "first principal axis" and is the eigenvector of matrix $\mathbf{C}$ with the largest eigenvalue $\lambda_1(\mathbf{v} = \mathbf{e}_1)$. The second principal axis corresponds to the unit vector $\mathbf{e}_2$, in which R has the second largest value and is perpendicular to $\mathbf{e}_1$ (and it is the eigenvector of $\mathbf{C}$ with the second largest eigenvalue λ_2). Likewise, the eigenvector $\mathbf{e}_i$ with the eigenvalue λ_i corresponds to the ith principal component axis, and the component of the conformation at t_a along the ith principal axis is given by a scalar product

$$c_i(t_a) = (\mathbf{X}(t_a) - \langle\mathbf{X}\rangle)\cdot\mathbf{e}_i \tag{41}$$

These components c_i can be used as the reaction coordinates for the free energy analyses below.

2.5. Computational Details. The peptide we considered in the present article is Met-enkephalin, and it has the amino acid sequence Tyr-Gly-Gly-Phe-Met. The peptide has 75 atomic sites (i.e., $N_S = 75$). The RISM-HNC equations and the replica-exchange method have been incorporated in the program KONF90.[34,35] A hybrid of the Newton−Raphson method and the Picard interaction strategy for solving the RISM equations have been employed as described in detail in ref 5. The conformational energy is based on ECEPP/2.[36−38] The peptide-bond dihedral angles ω were set equal to 180° for simplicity. The remaining dihedral angles ϕ and ψ in the main chain and χ in the side chains constitute the variables to be updated in the simulations (for Met-enkephalin the number of degrees of freedom is 19). One MC sweep consists of updating all of these angles once with Metropolis evaluation[39] for each update.

For the replica-exchange simulation, we used four replicas with four temperature values, 200, 298, 368, and 500 K. Before

TABLE 1: Temperature Dependence of the Solvent-Induced Potential E_T and the Solvent Free Energy E_{SOL} (kcal/mol) of the Conformations Obtained by Short Monte Carlo Simulations[a]

T(K)	CminT1	CminT2	CminT3	CminT4	CmaxT1	CmaxT2	CmaxT3	CmaxT4
200	102.1	103.1	103.7	106.2	109.4	113.4	118.7	122.0
	(87.9)	(92.3)	(86.6)	(88.8)	(92.0)	(94.3)	(90.6)	(97.7)
271	155.0	156.0	156.8	159.1	162.6	166.4	171.7	176.0
	(140.9)	(145.2)	(139.7)	(141.7)	(145.2)	(147.3)	(143.6)	(151.7)
368	219.2	220.1	221.2	223.4	227.2	230.7	235.9	241.5
	(205.1)	(209.3)	(204.1)	(206.0)	(209.7)	(211.6)	(207.8)	(217.2)
500	297.6	298.4	299.8	301.8	305.9	308.9	314.3	321.5
	(283.5)	(287.6)	(282.7)	(284.4)	(288.5)	(289.7)	(286.2)	(297.2)
E_C	14.1	10.8	17.1	17.4	17.4	19.1	28.1	24.3

[a] The lowest-energy (highest-energy) conformations obtained by short Monte Carlo simulations at 200, 271, 368, and 500 K are referred to as CminT1 (CmaxT1), CminT2 (CmaxT2), CminT3 (CmaxT3), and CminT4 (CmaxT4), respectively. E_C is the conformational energy (kcal/mol) of each structure. The solvent free energy E_{SOL} which is the value enclosed within parentheses is recalculated at each temperature (see eq 26). E_T is given by the sum of E_C and E_{SOL}.

taking the data, we made equilibration simulations of 5000 MC sweeps per replica. The total number of MC sweeps for the subsequent REM production run was 20 000 MC sweeps per replica. Replica exchange was tried every 20 MC sweeps.

3. Results and Discussion

3.1. Effectiveness of the Replica-Exchange Simulation. To estimate the required number of temperatures for the replica-exchange simulation, we first study the temperature dependence of the solvent-induced potential E_T in eq 1. Note that the solvation free energy E_{SOL} is temperature dependent (see eq 26), whereas the conformational energy E_C is independent of temperature. We checked the solvent-induced potential of some conformations at four temperatures. We chose the temperatures distributed exponentially between 200 and 500 K (i.e., $T_1 =$ 200 K, $T_2 = 271$ K, $T_3 = 368$ K, and $T_4 = 500$ K), following the optimal distribution found in ref 17. We performed short canonical MC simulations at four given temperatures and found the lowest-energy and highest-energy conformations at each temperature. In Table 1, the solvent-induced potential E_T and the solvent free energy E_{SOL} of these conformations at four temperatures are listed. The values of the solvent-induced potential in kcal/mol range from 102 to 122, from 155 to 176, from 219 to 242, and from 298 to 322, at 200, 271, 368, and 500 K, respectively. Thus, the solvent-induced potential at the four temperatures has no overlap in distributions. In the regular replica-exchange method, the histograms of the total energy distribution at neighboring temperatures need to overlap for replica exchange to occur (see eq 35). Therefore, at first sight, it seems that the number of temperatures chosen above (four) is too small. However, it turned out that the four temperatures were sufficient for ideal replica-exchange performances. The point is that we exchange replicas by using Δ in eq 34 instead of Δ of the regular replica-exchange method in eq 35, and E_T is almost proportional to temperature. This can be understood as follows. In Figure 1, we show the solvent-induced potential of these eight conformations as a function of temperature. $E_T(\boldsymbol{r}_C^{[i]},T)$ increases rapidly as temperature T increases and is almost proportional to temperature (see eq 26). This is due to the dominance of the entropic excluded-volume effects. The presence of a biomolecule generates a region where the solvent molecules cannot enter and decreases the total volume available to them. This causes a decrease in the solvent entropy, and the solvation free energy is governed by this entropic loss. As a result, $\beta\{E_T(\boldsymbol{r}_C^{[j]},T) - E_T(\boldsymbol{r}_C^{[i]},T)\}$ is almost temperature-independent. The magnitude of Δ in eq 34 is almost of 1 order of magnitude. The acceptance probability $\exp(-\Delta)$ in eq 36 is thus sufficiently large for the replica exchange to occur. In Table 2, this quantity calculated for a few pairs of conformations is listed. We see that at least one entry for each pair of neighboring temperatures is a finite value (>0.1). Hence, replica exchange is indeed possible between all of the pairs of neighboring temperatures.

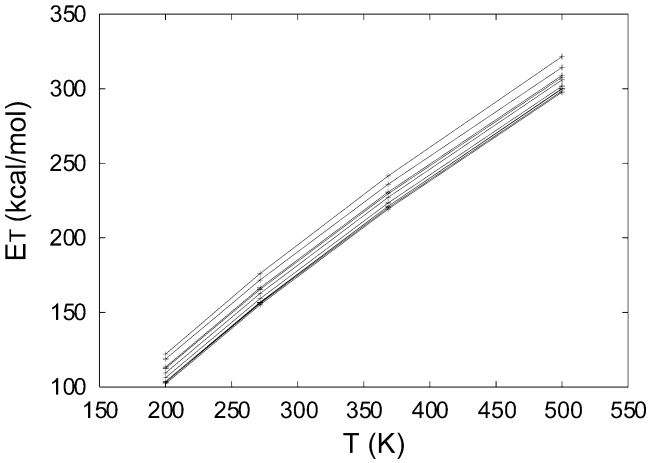

Figure 1. The solvent-induced potential E_T (kcal/mol) of eight conformations at four temperatures. Eight conformations were the lowest-energy and highest-energy conformations obtained by short Monte Carlo simulations at four temperatures. See also the caption of Table 1.

TABLE 2: Acceptance Probability $\exp(-\Delta)$ of Replica Exchange at Neighboring Temperatures

	CminT1	CmaxT1
CminT2	0.4435	0.9151
CmaxT2	0.0645	0.1331
	CminT2	CmaxT2
CminT3	0.0731	0.3026
CmaxT3	0.0069	0.0287
	CminT3	CmaxT4
CminT4	0.0300	0.1780
CmaxT4	0.0228	0.1353

The actual replica-exchange simulation was performed with four replicas at the four temperatures $T_m = 200$, 298, 368, and 500 K. We used the value 298 K instead of T_2 above (217 K) to include the room-temperature value. In Figure 2, the time series of the temperature label m and of the solvent-induced potential E_T for one of the replicas are shown. We see that this replica takes every temperature value and randomly walks in temperature space as expected (Figure 2a). Correspondingly, this replica undergoes a random walk in energy space (Figure

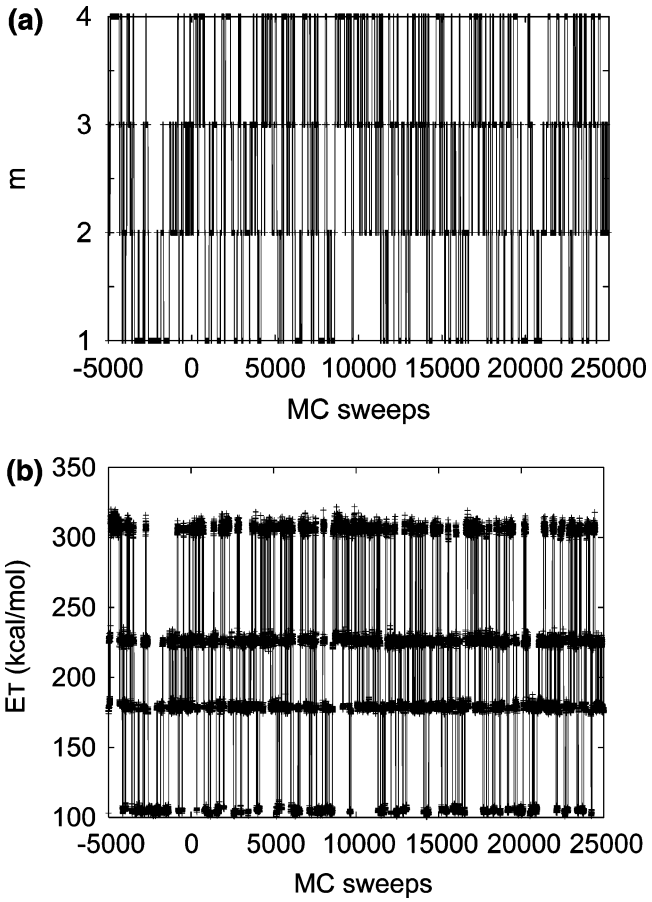

Figure 2. Time series of the temperature label m (a) and of the solvent-induced potential E_T (b) for one of the replicas. The negative values of MC sweeps correspond to the part of equilibration.

TABLE 3: Acceptance Ratios of the Present Replica-Exchange Simulation

pair of temperatures (K)	acceptance ratio
200 ↔ 298	0.16
298 ↔ 368	0.29
368 ↔ 500	0.25

2b). Other replicas also exhibit similar behavior. In Table 3, we list the acceptance ratios of replica exchange. It is clear that they are of the same order of magnitude (the values vary between 16% and 29%). For an optimal performance of REM simulations, the acceptance ratios of replica exchange should be sufficiently uniform and large (>10%). We can see that the present REM simulation has indeed achieved an optimal performance.

In Figure 3, the time series of the solvent-induced potential at the four temperatures are shown. Moreover, the time series of conformational energy E_C and solvation free energy E_{SOL} at each temperature are shown in Figure 4. The solvent-induced potential at different temperatures seems to rapidly reach thermal equilibrium. However, when we see in detail the time series of the two component terms, the conformational energy term and the solvation free energy term, we find that the equilibration actually needs about 5000 MC sweeps for each term. Note that the temperature dependence of conformational energy is much less than that of solvation free energy.

In Figure 5, the histogram of solvent-induced potential distribution at each temperature is shown (see also Figure 3). We have found above that only four replicas were required for an optimal performance of the present replica-exchange simulation, although there are no overlaps between pairs of neighboring distributions. Hence, the present system requires fewer replicas than the case for replica-exchange molecular dynamics (MD) simulations with explicit water molecules. In the previous replica-exchange MD simulations of Met-enkephalin with explicit water molecules, 36 replicas, 24 replicas, and 16 replicas were required to realize random walks in temperature space from 200 to 700 K,[11] from 250 to 500 K,[10] and from 275 K to 419 K,[40] respectively.

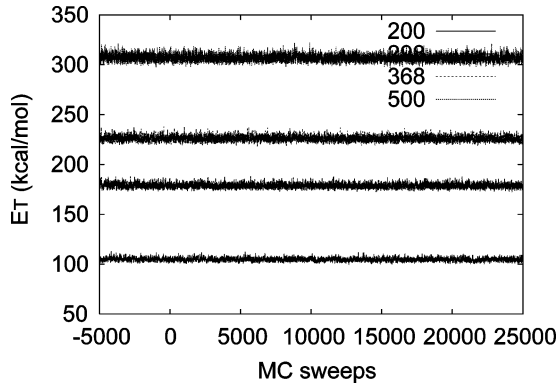

Figure 3. Time series of the solvent-induced potential at different temperatures. The negative values of the MC sweeps correspond to the part of equilibration.

TABLE 4: Backbone Dihedral Angles of the Lowest-Energy Conformations at 200 and 298 K

lowest-energy conformation at 200 K			lowest-energy conformation at 298 K		
residue	ϕ	ψ	residue	ϕ	ψ
1	−167.0	163.1	1	−152.3	167.4
2	−72.2	−141.6	2	−72.5	−137.0
3	70.1	96.6	3	74.2	128.1
4	−64.9	−40.9	4	−76.0	−30.2
5	−70.9	−89.7	5	−75.4	110.2

3.2. Lowest-Energy Conformations. We now consider the lowest-energy conformations of Met-enkephalin obtained by the present replica-exchange simulation in aqueous solution. We compare the lower-energy conformations obtained by the present simulation and those in the multicanonical simulations in the gas phase[42] and in aqueous solution based on the RISM theory.[24] The lowest-energy conformations obtained at 200 and 298 K are shown in Figures 6a and 6b, respectively. These conformations are fully extended. The results are in qualitatively good agreement with the observations in the NMR experiments,[41] which also imply fully extended conformations. The backbone dihedral angles of these conformations are listed in Table 4. The set of dihedral angles are quite similar to each other (except for those at the C-terminus).

In Figure 7, we show the lower-energy conformations obtained by the previous multicanonical simulations in the gas phase and in aqueous solution based on the RISM theory. Here, the previous multicanonical simulation in aqueous solution was based on the solvent-induced potential at a fixed temperature of 298 K.[24] In gas phase, we found that there were two dominant clusters of conformations at room temperature.[42] We see that the conformations in the gas phase form intrachain hydrogen bonds between the amide nitrogen and carbonyl oxygen in the backbone, which makes the structure compact. Especially, the lowest-energy conformation has two intrachain hydrogen bonds between glycine 2 and methionine 5 and forms a type II′ β turn involving Gly-Gly-Phe-Met (Figure 7a).[42] The second lowest-energy conformation has two intrachain hydrogen bonds be-

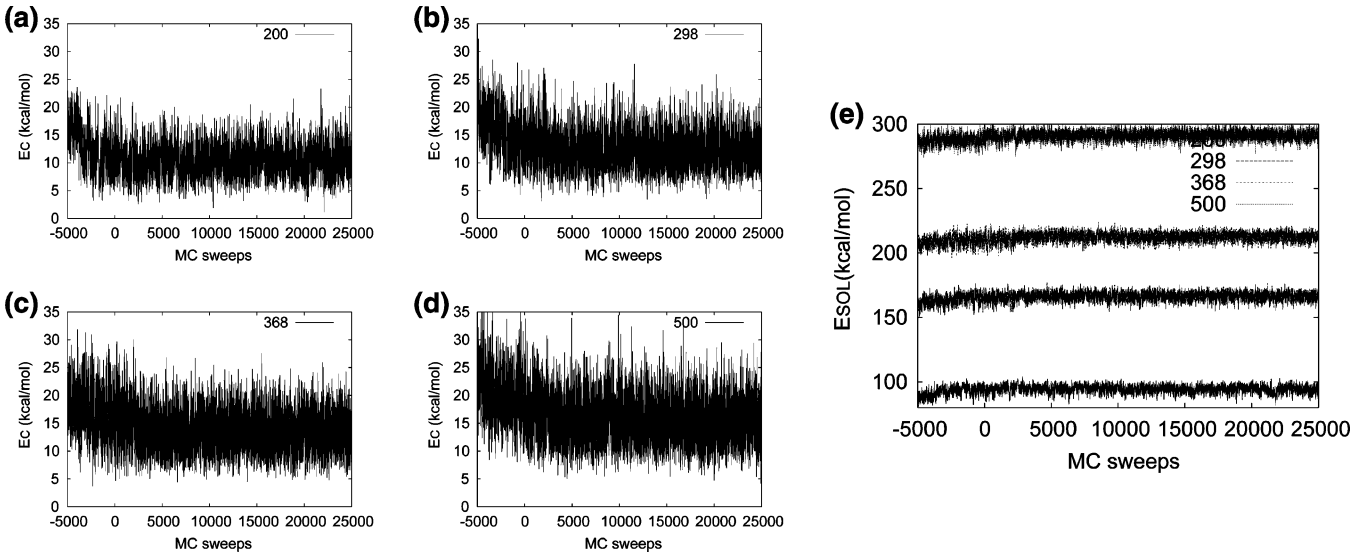

Figure 4. Time series of the conformational energy E_C (kcal/mol) at 200 K (a), 298 K (b), 368 K (c), and 500 K (d) and the solvation free energy E_{SOL} (kcal/mol) (e) at these four temperatures. The negative values of the MC sweeps correspond to the part of equilibration.

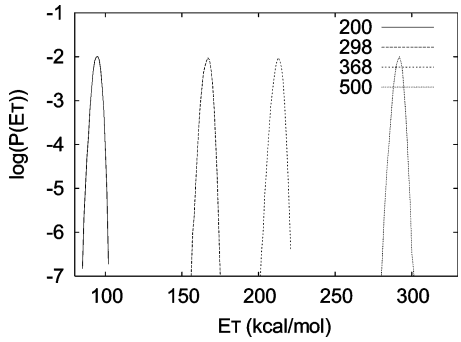

Figure 5. Probability distributions of the solvent-induced potential at the four temperatures.

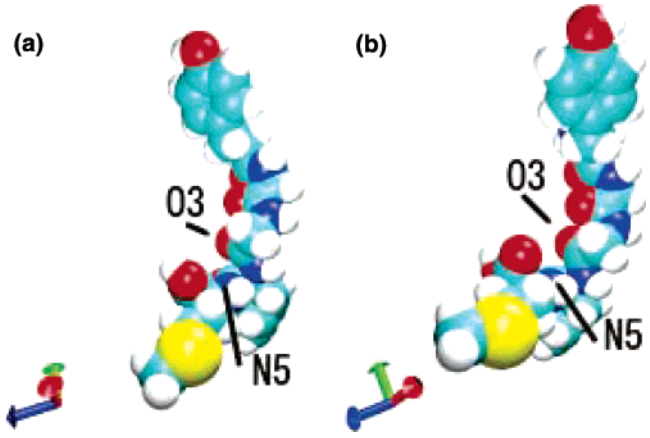

Figure 6. The lowest-energy conformations of Met-enkephalin obtained by the present replica-exchange simulation in aqueous solution at 200 K (a) and 298 K (b). O3 stands for the backbone oxygen atom of glycine 3, and N5 the backbone nitrogen atom of methionine 5. The figures were created with VMD[43] and Raster3D.[44]

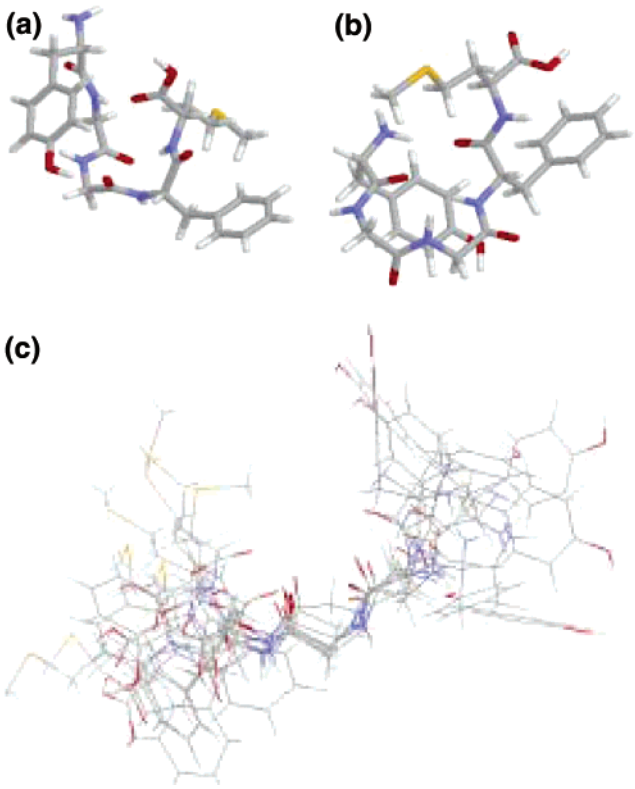

Figure 7. The lowest-energy (a) and second-lowest-energy (b) conformations of Met-enkephalin obtained by the previous multicanonical simulation in the gas phase[10] and the superposition of the eight representative low-energy conformations of Met-enkephalin obtained by the previous multicanonical simulation in aqueous solution[24] (c).

tween tyrosine 1 and phenylalanine 4 and forms a type I β turn involving Tyr-Gly-Gly-Phe (Figure 7b).[42] The lower-energy conformations in the gas phase are different from those in aqueous solution. In Figure 7c, the eight representative conformations obtained by the previous multicanonical simulation in aqueous solution[24] are shown. These are chosen from those in which the solvent-induced potential energy at 298 K was less than 174.0 kcal/mol and the root-mean-square distances of the backbone atoms from glycine 2 to phenylalanine 4 were larger than 0.4 Å. That is, we excluded similar structures with small root-mean-square distances from consideration. For the multicanonical simulation in aqueous solution, the eight conformations are also fully extended as in the present results in Figure 6.

The energy components of all of these conformations are listed in Table 5. The values of the solvent-induced potential at 200 K (REP1) and 298 K (REP2) are 99.8 and 172.1 kcal/mol, respectively. The values of the conformational energy of REP1

TABLE 5: Energy Components (kcal/mol) for the Lowest-Energy Conformations[a]

	E_T	E_C	E_{SOL}
REP1	99.8	12.3	87.5
REP2	172.1	11.2	160.9
MUL	172.2	11.6	160.6
MULGAS	−12.2	−12.2	

[a] The values were obtained by the previous multicanonical simulation in the gas phase (MULGAS), the previous multicanonical simulation in aqueous solution (MUL), and the present replica-exchange simulation in aqueous solution at 200 K (REP1) and 298 K (REP2).

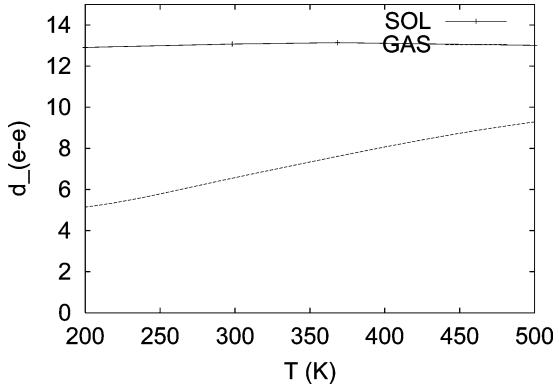

Figure 8. Average end-to-end distance of Met-enkephalin in aqueous solution (SOL) and in the gas phase (GAS) as a function of temperature. Here, the end-to-end distance is defined as the distance between the nitrogen atom at the N-terminus and the oxygen atom at the C-terminus. The results in aqueous solution are from the present replica-exchange simulation, and those in the gas phase are from the previous multicanonical simulation.[42]

and REP2 are similar to each other, whereas the solvation free energy values are different. Each energy component of REP2 is almost identical with that of MUL, reflecting the fact that the two cases correspond to the same temperature (298 K). The conformational energy of the lowest-energy conformation in gas phase is about −12 kcal/mol.[42] The conformational energy of the lowest-energy conformation in aqueous solution is about 10 kcal/mol, and it is much higher than that in gas phase.

3.3. Distribution Functions and Thermodynamic Quantities. We calculated the average end-to-end distance as a function of temperature by eq 20. Here, the end-to-end distance is defined as the distance between the nitrogen atom at the N-terminus and the oxygen atom at the C-terminus. The results are shown in Figure 8. The corresponding results in the gas phase[42] are also shown for comparison. The average end-to-end distance in aqueous solution at all temperatures stays around 13 Å; the conformations are extended in the entire temperature range. The results are similar to those in the previous multicanonical MC simulation with the RISM theory.[24] In the replica-exchange MD simulations with explicit water molecules (TIP3P model) which used AMBER parm 94 and AMBER parm 96 parameters, the average end-to-end distance for a wide range of temperatures (250−500 K) is about 10 and 12 Å, respectively.[10] Thus, these results are in accord with one another in the sense that the peptide is fully extended in water at all temperatures, although the values of the end-to-end distance are off by about 1 Å depending on the force fields. However, in the gas phase, the conformations are compact, and the average end-to-end distance is small at low temperatures due to intrachain hydrogen bonds, whereas the distance is large at high temperatures, because these intrachain hydrogen bonds are broken.

We calculated the pair distribution functions to study how the peptide is hydrated. In Figure 9, we show the distribution functions averaged over the different conformations of the peptide. The peaks in Figures 9a and 9b imply that the oxygen in the backbone of glycine 3 makes hydrogen bonds with water molecules. With an increase in temperature, the peaks become small as the hydrogen bonds become weak. The hydrogen bonds between the atoms in the peptide and those in the water molecules force the peptide to be extended. The pair distribution functions between the backbone nitrogen atom of methionine 5 and atoms in water (as shown in Figure 9, parts c and d) do not have pronounced peaks. This is because this nitrogen atom is buried among other backbone atoms without direct contact with water molecules (Figure 6, parts a and b).

We next study the correlation between the conformational energy and the solvation free energy. The results are shown in

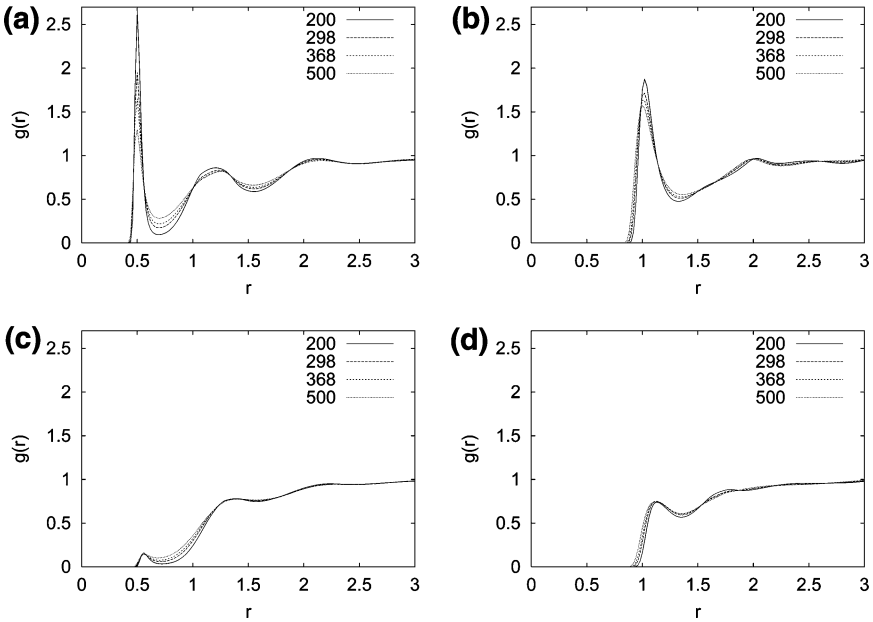

Figure 9. The pair distribution functions between backbone atoms and water atoms averaged over the different conformations of the peptide at each temperature. The pair distribution function between the oxygen atom in the backbone of the third residue and hydrogen atom (a) or oxygen atom (b) in water. The pair distribution function between the nitrogen atom in the backbone of the fifth residue and hydrogen atom (c) or oxygen atom (d) in water. These two atoms in the backbone are labeled as O3 and N5 in Figure 6.

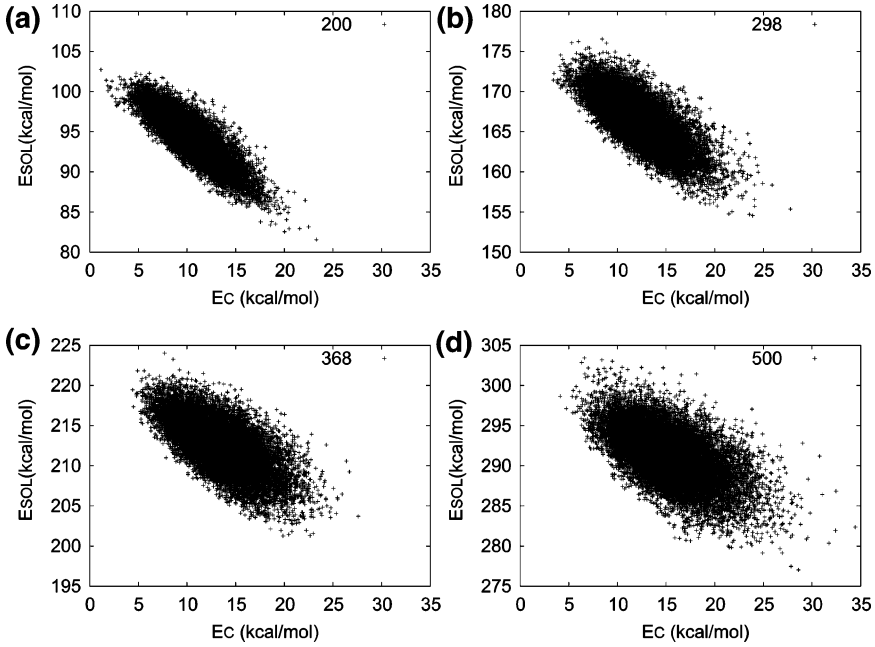

Figure 10. The relation between conformational energy and solvation free energy at 200 K (a), 298 K (b), 368 K (c), and 500 K (d).

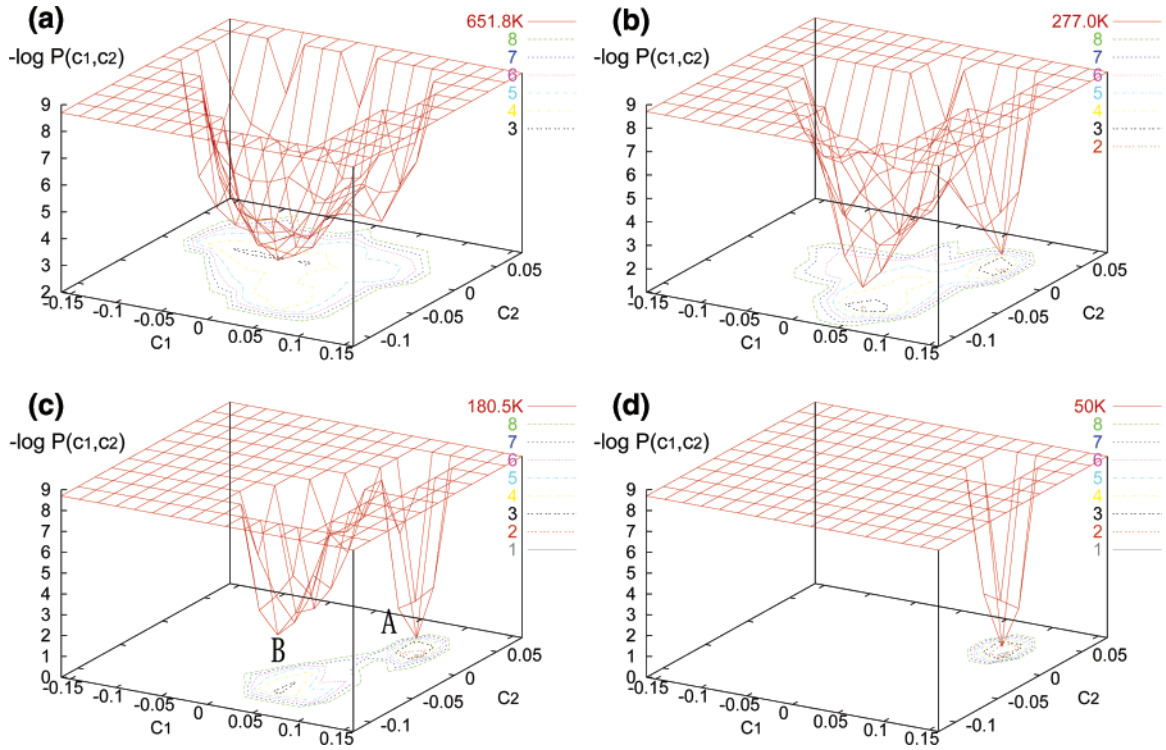

Figure 11. Free energy landscape of Met-enkephalin in gas phase (in units of k_BT) at 651 K (a), 277 K (b), 181 K (c), and 50 K (d) with respect of the first and second principal axes. The local minima A and B correspond to the lowest-energy and the second-lowest-energy states, respectively.

Figure 10. We find a clear inverse correlation between the conformational energy and the solvation free energy for a wide range of temperatures. This tendency becomes more pronounced as the temperature is lowered. The competition between the conformational energy and the solvation free energy occurs in aqueous solution.

3.4. Free Energy Surfaces in the Gas Phase and in Aqueous Solution. We now examine the free energy surfaces in the gas phase and in aqueous solution by principal component analysis. As for the gas-phase results, we used the data from the previous replica-exchange simulation.[10,20,21] In this simulation, eight replicas with eight different temperatures, 50, 77, 118, 181, 277, 425, 652, and 1000 K, were used. For the principal component analysis, 6000 structures were taken from the trajectories at 50, 181, 277, 425, and 652 K. The total number of data points is thus 30 000, and these data were used to determine the principal axes. However, for the analysis in aqueous solution, we used 5000 conformations from the trajectories at the four temperatures (i.e., 20 000 conformations altogether), and the principal axes were determined using these conformations. In both cases, we only used the coordinates of backbone atoms and set the mass weight to 1 for all backbone atoms.

We now study the free energy landscapes (potential of mean force) in the PCA space. In Figure 11, the free energy landscapes in the gas phase with respect to the first and second principal

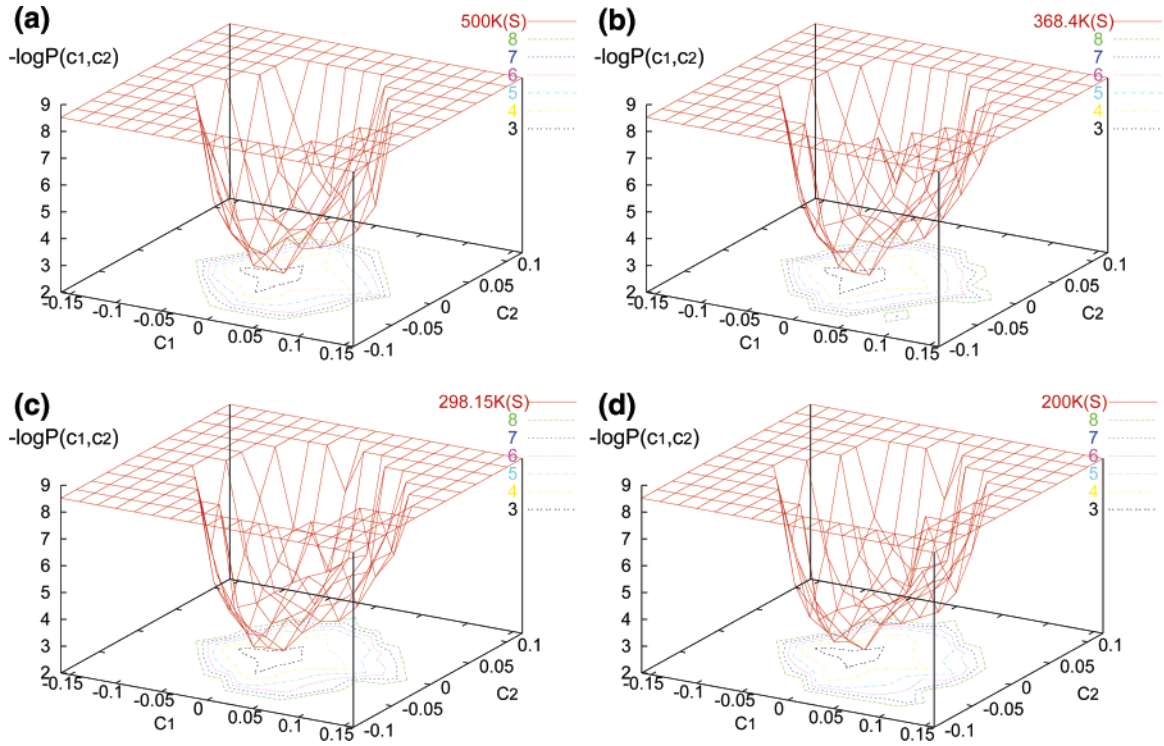

Figure 12. Free energy landscape of Met-enkephalin in aqueous solution (in units of k_BT) at 500 K (a), 368 K (b), 298 K (c), and 200 K (d) with respect of the first and second principal axes.

axes are shown. Here, the free energy (potential of mean force) is defined by

$$F(c_1,c_2,T) = -k_B T \ln P(c_1,c_2,T) \tag{42}$$

where $P(c_1,c_2,T)$ is the probability at temperature T to find the peptide conformation with values c_1 and c_2, which are the components of conformations along the first principal axis and the second principal axis, respectively (see eq 41). At the highest temperature, there are many configurations. The free energy surface is spread broadly, and there is no high energy barrier. As the temperature is decreased, some local minima appear. At 181 K, the minima at A and B in Figure 11c, which respectively correspond to the lowest-energy conformation and the second lowest-energy conformation, are dominant. The free energy barrier between clusters A and B is high. At the lowest temperature, only cluster A appears. In Figure 12, energy landscapes in aqueous solution at four temperatures are shown. The free energy surfaces in aqueous solution are parabolalike and smooth for a wide range of temperatures. We see that the shapes of energy surfaces are very similar, and there are no energy barriers unlike those in gas phase. Hence, the existence of water drastically smoothes out the free energy landscapes. In ref 40, the free energy landscape of Met-enkephalin was also obtained by the replica-exchange MD simulation with explicit water molecules. Four predominant configurations were identified at $T = 225$ K with the AMBER parm 94 force field. Two of them correspond to helical conformations, and the other two correspond to coil structures. However, only one dominant configuration (coil) was obtained at $T = 275$ K with the AMBER parm 96 force field. Our results with the ECEPP/2 potential energy function and RISM solvation theory are similar to the latter results in the sense that we observe only one local-minimum configuration with extended coil configurations without the formation of helices. It is now well-known that the AMBER parm 94 forms α-helix conformations too much (for instance, see ref 45). Because the results strongly depend on the choice of force fields employed, it is difficult to extract quantitative results. However, the effects of solvent seem to be that the peptide tends to be extended more than in gas phase and that the free energy landscape is smoother than that found in gas phase[8,11,40]

4. Conclusions

We have performed the modified replica-exchange simulation of Met-enkephalin in aqueous solution. The solvent effects were incorporated by the reference interaction site model theory. It was found that the existence of solvent tends to extend the peptide configuration and smoothes out the free energy landscape.

The problem of regular replica-exchange simulations lies in the fact that as the system size becomes larger, a great number of replicas are required, resulting in large increase of computation time. The required number of replicas undergoes a remarkably large increase when a simulation in solvent is undertaken. In the case of Met-enkephalin, for example, more than 16 replicas were required in water to guarantee sufficiently high replica-exchange frequency.[10,11,40] For the C-peptide of ribonuclease A (13 residues) in water, the simulation was performed using 32 replicas.[46] In the present case of a hybrid method applied to Met-enkephalin in aqueous solution, four replicas were sufficient to guarantee high replica-exchange frequency. The number of replicas is reduced when the peptide molecule is immersed in water, which is in marked contrast with the case of the usual simulation. We ascribed this to the dominance of the entropic excluded-volume effects. This advantage should hold for other biomolecules as long as their hydrophobicity is sufficiently high.

Acknowledgment. The simulations were performed on the computers at the Research Center for Computational Science, Okazaki National Research Institute. This work was supported, in part, by the Grants-in-Aid for Scientific Research on Priority

Areas "Genome Information Science" and "Water and Biomolecules", for Young Scientists (B), 14740170, 2002, and for the NAREGI Nanoscience Project from the Ministry of Education, Culture, Sports, Science and Technology, Japan.

References and Notes

(1) Privalov, P. L.; Griko, Y. V.; Venyaminov, S. Y.; Kutyshenko, V. P. *J. Mol. Biol.* **1986**, *190*, 487−498.
(2) Chandler, D.; Andersen, H. C. *J. Chem. Phys.* **1972**, *57*, 1930−1937.
(3) Hirata, F.; Rossky, P. J. *Chem. Phys. Lett.* **1981**, *83*, 329−334.
(4) Perkyns, J.; Pettitt, B. M. *Chem. Phys. Lett.* **1992**, *190*, 626−630.
(5) Kinoshita, M. In *Molecular Theory of Solvation*; Hirata, F., Ed.; Kluwer Academic: Dordrecht, 2003; pp 101−168.
(6) Kinoshita, M.; Okamoto, Y.; Hirata, F. *J. Comput. Chem.* **1997**, *18*, 1320−1326. Kinoshita, M.; Okamoto, Y.; Hirata, F. *J. Comput. Chem.* **1998**, *19*, 1724−1735.
(7) Kinoshita, M.; Okamoto, Y.; Hirata, F. *J. Chem. Phys.* **1997**, *107*, 1586−1599.
(8) Kinoshita, M.; Okamoto, Y.; Hirata, F. *J. Am. Chem. Soc.* **1998**, *120*, 1855−1863.
(9) Kinoshita, M.; Okamoto, Y.; Hirata, F. *J. Chem. Phys.* **1999**, *110*, 4090−4100.
(10) Mitsutake, A.; Sugita, Y.; Okamoto, Y. *Biopolymers* **2001**, *60*, 96−123.
(11) Sugita, Y.; Okamoto, Y. In *Lecture Notes in Computational Science and Engineering*; Schlick, T., Gan, H. H., Eds.; Springer-Verlag: Berlin, 2002; pp 304−332. Sugita, Y.; Okamoto, Y. *Condensed Matter*, published online Feb 16, 2001, http://arxiv.org/abs/cond-mat/0102296.
(12) Berg, B. A.; Neuhaus, T. *Phys. Lett.* **1991**, *B267*, 249−253.
(13) Berg, B. A.; Neuhaus, T. *Phys. Rev. Lett.* **1992**, *68*, 9−12.
(14) Hukushima, K.; Nemoto, K. *J. Phys. Soc. Jpn.* **1996**, *65*, 1604−1608.
(15) Hukushima, K.; Takayama, H.; Nemoto, K. *Int. J. Mod. Phys.* **1996**, *C7*, 337−344.
(16) Geyer, C. J. *Computing Science and Statistics: Proc. 23rd Symp. on the Interface*, Keramidas, E. M., Ed.; Interface Foundation: Fairfax Station, 1991; p 156.
(17) Sugita, Y.; Okamoto, Y. *Chem. Phys. Lett.* **1999**, *314*, 141−151.
(18) Sugita, Y.; Kitao, A.; Okamoto, Y. *J. Chem. Phys.* **2000**, *113*, 6042−6051.
(19) Sugita, Y.; Okamoto, Y. *Chem. Phys. Lett.* **2000**, *329*, 261−270.
(20) Mitsutake, A.; Okamoto, Y. *Chem. Phys. Lett.* **2000**, *332*, 131−138.
(21) Mitsutake, A.; Sugita, Y.; Okamoto, Y. *J. Chem. Phys.* **2003**, *118*, 6664−6675.
(22) Mitsutake, A.; Sugita, Y.; Okamoto, Y. *J. Chem. Phys.* **2003**, *118*, 6676−6688.
(23) Mitsutake, A.; Okamoto, Y. *J. Chem. Phys.* **2004**, *121*, 2491−2504.
(24) Mitsutake, A.; Kinoshita, M.; Okamoto, Y.; Hirata, F. *Chem. Phys. Lett.* **2000**, *329*, 295−303.
(25) LaPenna, G.; Mitsutake, A.; Masuya, M.; Okamoto, Y. *Chem. Phys. Lett.* **2003**, *380*, 609−619.
(26) Kitao, A.; Hirata, F.; Go, N. *Chem. Phys.* **1991**, *158*, 447−472.
(27) Abagyan, R.; Argos, P. *J. Mol. Biol.* **1992**, *225*, 519−532.
(28) Garcia, A. E. *Phys. Rev. Lett.* **1992**, *68*, 2696−2699.
(29) Amadei, A.; Linssen, A. B. M.; Berendsen, H. J. C. *Proteins* **1993**, *17*, 412−425.
(30) Hayward, S.; Kitao, A.; Hirata, F.; Go, N. *J. Mol. Biol.* **1993**, *234*, 1207−1217.
(31) Levy, R. M.; Srinivasan, A. R.; Olson, W. K.; McCammon, J. A. *Biopolymers* **1984**, *23*, 1099−1112.
(32) Berendsen, H. J. C.; Grigera, J. R.; Straatsma, T. P. J. *J. Phys. Chem.* **1987**, *91*, 6269−6271.
(33) Singer, S. J.; Chandler, D. *Mol. Phys.* **1985**, *55*, 621−625.
(34) Kawai, H.; Okamoto, Y.; Fukugita, M.; Nakazawa, T.; Kikuchi, T. *Chem. Lett.* **1991**, 213−216.
(35) Okamoto, Y.; Fukugita, M.; Nakazawa, T.; Kawai, H. *Protein Eng.* **1991**, *4*, 639−647.
(36) Momany, F. A.; McGuire, R. F.; Burgess, A. W.; Scheraga, H. A. *J. Phys. Chem.* **1975**, 79, 2361−2381.
(37) Némethy, G.; Pottle, M. S.; Scheraga, H. A. *J. Phys. Chem.* **1983**, *87*, 1883−1887.
(38) Sippl, M. J.; Némethy, G.; Scheraga, H. A. *J. Phys. Chem.* **1984**, *88*, 6231−6233.
(39) Metropolis, N.; Rosenbluth, A. W.; Rosenbluth, M. N.; Teller, A. H.; Teller, E. *J. Chem. Phys.* **1953**, *21*, 1087−1092.
(40) Sanbonmatsu, K. Y.; Garcia, A. E. *Proteins* **2002**, *46*, 225−234.
(41) Graham, W. H.; Carter, S. E., II; Hickes, P. R. *Biopolymers* **1992**, *32*, 1755−1764.
(42) Mitsutake, A.; Hansmann, U. H. E.; Okamoto, Y. *J. Mol. Graph. Mod.* **1998**, *16*, 226−238.
(43) Humphrey, W.; Dalke, A.; Schulten, K. *J. Mol. Graphics* **1996**, *14.1*, 33−38.
(44) Merritt, E. A.; Bacon, D. J. *Meth. Enzymol.* **1997**, *277*, 505−524
(45) Yoda, T.; Sugita, Y.; Okamoto, Y. *Chem. Phys. Lett.* **2004**, *386*, 460−467.
(46) Sugita, Y.; Okamoto, Y. Submitted.